Anderson disorder related p-type conductivity and metal-insulator transition in β-Ga2O3

Zeyu Chi, Se-Rim Park, Luka Burdiladze, Tamar Tchelidze, Jean-Michel Chauveau, Yves Dumont, Sang-Mo Koo, Zurab Kushitashvili, Amiran Bibilashvili, Gérard Guillot, et al.

Materials Today Physics 49 (2024) 101602

Contents lists available at ScienceDirect

Materials Today Physics

journal homepage: www.journals.elsevier.com/materials-today-physics

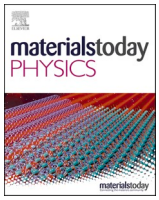

Anderson disorder related *p*-type conductivity and metal-insulator transition in β-Ga_2O_3

Zeyu Chi [a], Se-Rim Park [a,b], Luka Burdiladze [c], Tamar Tchelidze [c], Jean-Michel Chauveau [a], Yves Dumont [a], Sang-Mo Koo [b], Zurab Kushitashvili [d], Amiran Bibilashvili [d], Gérard Guillot [e], Amador Pérez-Tomás [f,g], Xin-Ying Tsai [h], Fu-Gow Tarntair [h], Ray Hua Horng [h,**], Ekaterine Chikoidze [a,*]

[a] Université Paris-Saclay, UVSQ- CNRS, Groupe D'Etude de la Matière Condensée (GEMaC), 45 Av. des Etats-Unis, 78035, Versailles Cedex, France
[b] Department of Electronic Materials Engineering, Kwangwoon University, Seoul, 01897, Republic of Korea
[c] Faculty of Exact and Natural Science, Department of Physics, Ivane Javakhishvili Tbilisi State University, 3 Av. Tchavtchavadze, 0179, Tbilisi, Georgia
[d] Institute of Micro and Nanoelectronics, Tbilisi, Georgia
[e] Univ. Lyon, CNRS, ECL, UCBL, INSA Lyon, CPE, Institut des Nanotechnologies de Lyon, 69621, Villeurbanne, Cedex, France
[f] Catalan Institute of Nanoscience and Nanotechnology (ICN2), CSIC and the Barcelona Institute of Science and Technology, Barcelona, Spain
[g] Institute of Microelectronics of Barcelona (IMB-CNM-CSIC), C/ Dels Til.lers s/n, Campus UAB, Bellaterra, 08193, Barcelona, Spain
[h] Institute of Electronics, National Yang Ming Chiao Tung University, Hsinchu, 30010, Taiwan, Taiwan, ROC

A B S T R A C T

The *p*-type doping is one of the main challenges of the emerging semiconductor β-Ga_2O_3 technology. Phosphorus (P) implantation has been recently reported as a novel route to achieve *p*-type conduction on Ga_2O_3 at room temperature. Here, P-implanted epilayers, grown onto *c*-plane sapphire revealed a pseudo-metallic behavior (ρ = 1.3–0.3 Ω cm) in the 300–600 K range with a hole carrier concentration of $p \sim 4$–6×10^{18} cm^{-3} and hole mobility of μ = 1.2–2.1 $cm^2/(V{\cdot}s)$. At sufficiently low temperature, a metal-insulator transition arises together with an increase in the positive magnetoresistance, reaching up to 200 % (9 T) large positive magneto resistance effect at 2 K. It is suggested that an Anderson delocalization model explains the room temperature conduction, and the transition to an insulator state caused by random variation of potential related to the incorporated phosphorous in Ga_2O_3. We believe that the lack of shallow acceptors can be mitigated by promoting Anderson disorder through the incorporation of a high level of acceptor impurities.

1. Introduction

Gallium oxide (Ga_2O_3) is an ultra-wide band gap oxide semiconductor that has recently attracted considerable attention owing to its outstanding material properties. Among its five polymorphs (α, β, γ, δ, and ε), the monoclinic β-phase is the most thermodynamically stable one, it exhibits an ultra-wide band gap of 4.6–4.9 eV with predicted high breakdown electrical field larger than 8 MV/cm [1,2]. In addition, the Ga_2O_3 semiconductor technology is becoming very successful with commercial available 6-inch wafers and an excellent control of the *n*-type doping concentration in the range of 10^{16}–10^{20} cm^{-3} [3–7]. These properties make this material attractive for opto-electronics (e.g. deep UV photodetector [8]) and power electronics (e.g. field effect transistors [9,10], Schottky barrier diode [11] or *p*-NiO/*n*-Ga_2O_3 heterojunction diode [12,13]). However, despite the significant progress in developing *n*-type Ga_2O_3, achieving reliable and efficient *p*-type conductivity remains a critical challenge, limiting the development of bipolar devices such as *p*-*n* junctions, which are essential for realizing the full potential of Ga_2O_3-based electronic devices.

The difficulty of achieving *p*-type conductivity in β-Ga_2O_3 is primarily due to its wide bandgap and the deep native acceptor levels and consequently of acceptor dopants. The origin of the free holes in native *p*-Ga_2O_3 was attributed to the Ga vacancies with ionization energy E_i = 1.12 eV [14,15]. The probability for achieving *p*-type or *n*-type conductivity in wide band gap materials through external impurity incorporation depends on the electronic states of native point defects and position relative to the valence and conduction bands [16]. Several elements such as Zn [1,17], N [18,19] and even complex-like defects $N_O - V_{Ga}$ [20], $V_O - Zn_{Ga}$ [21] have been demonstrated playing the role of active acceptors leading *p*-type conductivity in Gallium oxide.

* Corresponding author.
** Corresponding author.
E-mail addresses: rayhua@nycu.edu.tw (R.H. Horng), Ekaterine.chikoidze@uvsq.fr (E. Chikoidze).

https://doi.org/10.1016/j.mtphys.2024.101602
Received 12 July 2024; Received in revised form 14 October 2024; Accepted 19 November 2024
Available online 20 November 2024

Phosphorus (P) implantation has recently attracted significant attention as a potential strategy for achieving effective *p*-type doping in β-Ga_2O_3. Although theoretical predictions suggest that phosphorus doping may not provide shallow acceptors in β-Ga_2O_3 (with an energy level of E_V + 0.55 eV in N-P co-doping) [22], experimental work by Horng et al. demonstrated hole conductivity at room temperature in phosphorus-ion implanted β-Ga_2O_3 thin films grown on *c*-plane sapphire substrates [23]. After rapid thermal annealing (RTA), Horng et al. also reported a shift in the β-Ga_2O_3 (−603) diffraction peak to a higher angle (58.93°) compared to the unintentionally doped (UID) layer, suggesting a reduction in *d*-spacing due to phosphorus substituting oxygen [24]. Supporting this, Li et al., through *ab-initio* simulations, observed that the Ga–P bonds exhibit more covalent character and greater stability than the corresponding Ga–O bonds, proposing a potential approach to mitigate the trapping effects caused by oxygen vacancies [22]. As there are two positions for oxygen, these bonds are referred as Ga_1-P_1 and Ga_2-P_2. The bond lengths of Ga_1-P_1 (>1.960 Å) and Ga_2-P_2 (>2.019 Å) for P-doped β-Ga_2O_3, are larger than that of Ga_2-O_2 (1.912 Å) and Ga_2-O_1 (1.984 Å).

In this work, the implanted phosphorus concentration was 8×10^{19} cm^{-3}, the room-temperature resistivity, hole concentration and the Hall hole mobility were 9.7 Ω cm, 1.6×10^{18} cm^{-3}, and 0.4 $cm^2/(V{\cdot}s)$, respectively. Based on the first-principles Density Functional Theory (DFT), the oxidation state of phosphorus ions affects their likelihood of incorporation into the β-Ga_2O_3 lattice as defects, but also influences the Fermi level's position [23]. Consequently, using the phosphorus-ions implantation technology, homoepitaxial *p-n* β-Ga_2O_3 junction grown on sapphire substrate was recently demonstrated [24]. However, there is still a lack of comprehensive understanding regarding how phosphorus incorporation influences the electrical and transport properties of β-Ga_2O_3.

In this study, we aim to clarify the effect of P incorporation on the electrical transport properties of the P implanted β-Ga_2O_3 [23]. Mainely, we examine the influence of phosphorus incorporation on carrier concentration, mobility, and magnetoresistance, discussing our findings in the context of the Anderson localization model for disordered systems.

2. Results and discussion

2.1. Phosphorus implanted β-Ga_2O_3 thin films

β-Ga_2O_3 epilayers were grown at 875 °C on *c*-plane (0001) sapphire substrate by Metal-Organic Chemical Vapor Deposition (MOCVD) – see experimental detail section. The thickness of the β-Ga_2O_3 epilayer was estimated to be 175 nm by secondary-ion mass spectrometry (SIMS). As-grown samples were subsequently implanted at different energies and doses to obtain box profile distribution of implanted phosphorus ions followed by a rapid thermal annealing (RTA) at 1100 °C for 1 min in a N_2 environment. Table 1 summarizes the doses for samples #1 and #2, the corresponding incorporated phosphorus ion concentrations were determined by SIMS to be 8×10^{19} cm^{-3} and 2×10^{19} cm^{-3}, respectively.

Fig. 1 (a) shows X-ray diffraction (XRD) out-of-plane θ−2θ scan of two phosphorus implanted and unintentionally doped (UID) β-Ga_2O_3 thin films grown on *c*-plane sapphire substrate. The peaks labeled by "*" indicate XRD reflections corresponding to the *c*-sapphire substrate. For both samples, three peaks are observed at 2θ values of around 38.16°, 58.84°, and 82.06°, corresponding to monoclinic β-Ga_2O_3 (−402), (−603), and (−804), respectively, indicating a preferential (−201) orientation. These main peaks are zoomed as shown in Fig. 1 (b), revealing that the lattice parameters of the samples with different doses of phosphorus ions implantation are comparable. Surface morphology of the Ga_2O_3 epilayers was analyzed using atomic force microscopy (AFM), revealing a notable difference between the two samples. Sample #2, with a lower implantation dose ($1.95 \times 10^{14}/cm^2$), exhibited reduced surface roughness (1.38 nm) compared to Sample #1 ($7.8 \times 10^{14}/cm^2$, 1.9 nm). Moreover, fewer deep regions were observed in Sample #2, indicating less surface damage. Detailed AFM images are provided in Supplementary file (Fig. S1). Fig. 1 (c) shows the optical band gaps determined from a classical Tauc's plot extrapolation. The absorption coefficients (α) were calculated from reflectance and transmittance measurements at room temperature, in the 200–850 nm wavelength range. The optical bandgap was found at $E_g = 4.77 \pm 0.06$ and 4.87 ± 0.07 eV for samples #1 and #2, respectively.

Table 1
Implantation doses for samples #1 and #2.

Sample		#1	#2
Dose (cm^{-2})	100 keV	6.4×10^{14}	1.6×10^{14}
	50 keV	4×10^{13}	1×10^{13}
	40 keV	1×10^{14}	2.5×10^{13}
Total dose (cm^{-2})		7.8×10^{14}	1.95×10^{14}

Electrical metal contacts Ni/Au (20/100 nm) were deposited onto the corners of the square-shape sample, followed by RTA at 600 °C in a N_2 environment for 1 min. Fig. 2 (a) shows the measured room temperature forward current density-voltage (*J-V*) characteristics for sample #1 (black curve) and #2 (red curve). For both samples, Ni/Au form Ohmic contacts to the P implanted Ga_2O_3 layers, displaying quite similar behavior (current density $J = 11.0$ and 10.3 mA/cm^2 for samples #1 and #2 at 10 V, respectively). The work function of sample #2 was measured using a Kelvin probe. Acquisitions were taken at the center and at the edge of the sample surface. The measured work functions were of 4.8305 eV and 4.8503 eV, respectively. TCAD simulations were carried out with a thermionic emission (TE) model (Fig. 2 (a) blue curve) using SILVACO-Atlas (input parameters are given in the experimental details section). The differences between simulation experimental (e.g., $J = 3.2$ mA/cm^2 at 10 V) can be attributed to several factors such as the surface states on Ga_2O_3 film, and the effective density of states at the valence band [25,26].

2.2. Electrical and magneto-transport properties

According to the *J-V* characteristics shown above and the Hall effect measurements performed at room temperature, samples #1 and #2 exhibit similar electrical transport properties. Therefore, we will focus further analysis on samples #1. The Hall voltage increases linearly with applied external magnetic field (Fig. 3 (a)), indicating that free holes are the dominant carriers. The resistivity, hole Hall mobility, and the hole concentration were measured to be $\rho = 1.3$ Ω cm, $\mu = 1.2$ $cm^2/(V{\cdot}s)$, and $p = 4.4 \times 10^{18}$ cm^{-3}, respectively. The measured free carrier concentration is significantly lower than incorporated phosphorus concentration ($N_A = 8 \times 10^{19}$ cm^{-3}), suggesting a high compensation ratio via donors if all phosphorus ions occupy the equivalent substitutional oxygen site [22,27]. Alternatively, it is possible that only a fraction of phosphorus substitutes for oxygen, while the others occupy different sites and are not playing role of an activated acceptor. In both cases, sample can be considered as strongly compensated.

As shown in Fig. 2 (b), the *J-V* curves remain comparable in the temperature range of 300–550 K, coherently to slight change of resistivity observed above room temperature shown in Fig. 3 (b). Indeed, the measured values of resistivity, hole Hall mobility, and the hole concentration at 600 K are $\rho = 0.33$ Ω·cm, $\mu = 2.06$ $cm^2/(V{\cdot}s)$, and $p = 6.5 \times 10^{18}$ cm^{-3}, respectively. Hole concentration does not vary significantly above room temperature. The slight change in resistivity is attributed to the variations in mobility values due to carrier scattering. Based on these results, the conductivity can be attributed to an impurity band created by the phosphorus acceptors.

To further study the conduction mechanism, the low temperature electrical measurements were performed using a Physical Property Measurement System (PPMS from Quantum Design) (Fig. 4). Note that the metal contacts were prepared by silver paste in four-point aligned

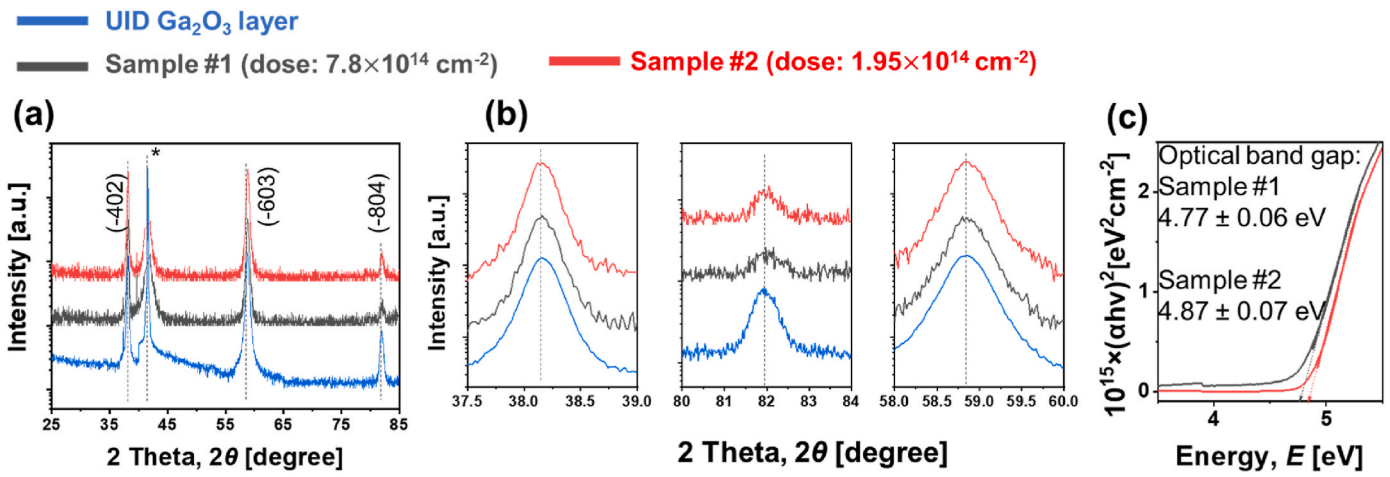

Fig. 1. (a) XRD patterns of UID and phosphorus implanted β-Ga_2O_3 thin films on *c*-plane sapphire substrate in the range of $2\theta = 25–85°$. (b) Zoomed 2θ peaks of β-Ga_2O_3. (c) Optical bandgap determination.

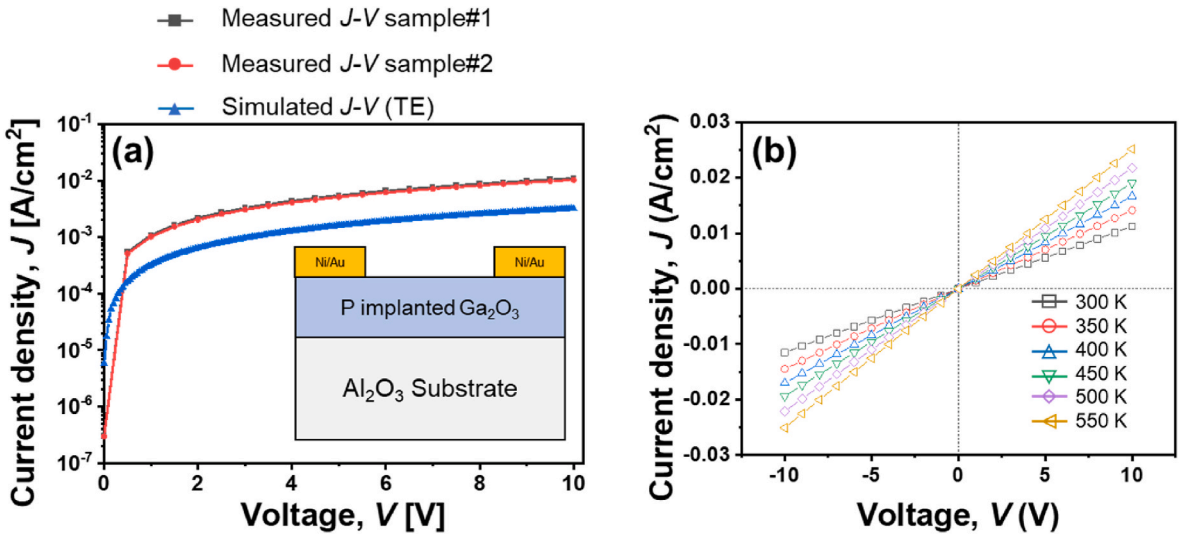

Fig. 2. (a) Measured *J-V* characteristics along with the simulated data. The blue line corresponds to the simulated curve based on the TE model. (b) The *J-V* curves as a function of temperature from 300 to 550 K for sample #1.

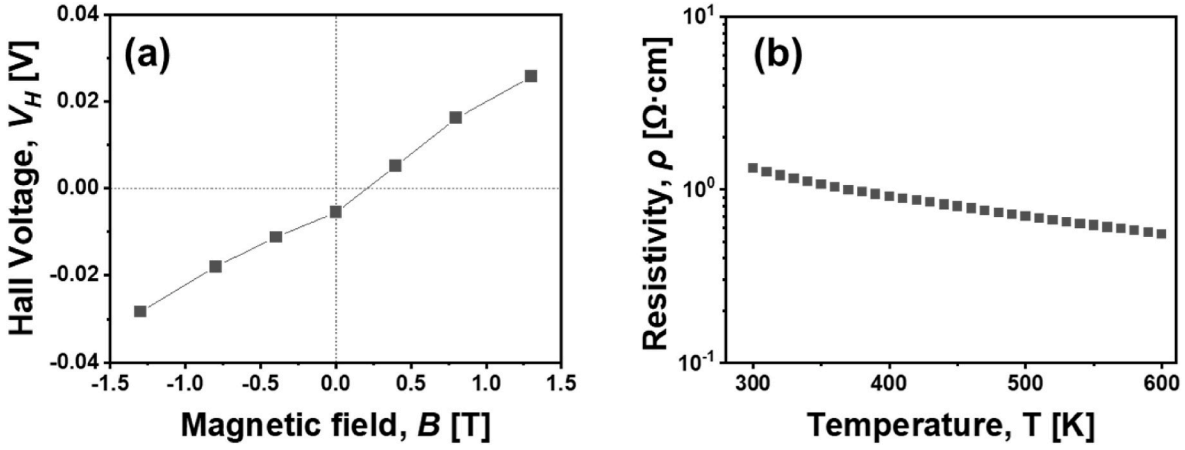

Fig. 3. (a) Hall voltage as a function of perpendicularly applied magnetic field from −1.6 - +1.6 T, at 300 K, indicating that the layer is *p*-type. (b) Temperature-dependent resistivity in the 300–600 K temperature range.

configuration. The *I-V* characteristics were tested and, surprisingly, they remained linear down to 5 K in the range of -10 - +10 V (Fig. 4 (a)), showeda quasi-linear behavior at 2 K (Fig. 4 (b)). The resistance increases by almost four orders of magnitude as the temperature decreased from 300 to 2 K (from $R = 200$ kΩ to $R = 1$ GΩ), with a sharp rise in resistance at $T < 30$ K (Fig. 4 (c)), corresponding to an impurity band related "metal" to insulator transition. At very low temperatures, the dominant conduction mechanism is variable range hopping (VRH) conduction. A variable range hopping regime (VRH) is a temperature-dependent conduction mechanism where carriers hop between localized states over variable distances, rather than strictly to the nearest neighbor sites. Mott [28] proposed that, at low temperatures, the hopping between nearest neighbor sites is not always favored as the levels may be significantly different in energy. In other words, carrier prefers to move to a more energetically favorable (i.e., the most efficient conduction path) site but may be spatially distant. In Mott's VRH, the conductivity is given by Refs. [28,29]:

$$\sigma(T) = \sigma_0 \, exp\left(-\frac{T_M}{T}\right)^{\frac{1}{n+1}}$$

where n is the dimensionality of the system ($n = 2$ for 2D system, while n becomes 3 for 3D sample), $T_M = \frac{18.1}{k_B N(Ef)\xi^3}$, ξ is a carrier localization length, T_M is Mott's characteristic temperature and $N(E_f)$ is the constant density of states at Fermi level [30]. Here, a slope of -17.2 $K^{1/4}$ was found by the plot (Fig. 4 (d)).

2.3. Magnetotransport

In addition to the electrical transport mechanism, magnetoresistance (*MR*) measurements have also been carried out. There are still relatively few reports on magnetoresistance effects in Ga_2O_3. Chikoidze et al. analyzed the *MR* of Sn doped α-Ga_2O_3 thin films, observing that the *MR* behavior varies with different doping level ranging from 10^{18} to 10^{20} cm^{-3} [4]. Positive longitudinal *MR* in quadratic shape was observed in Si doped β-Ga_2O_3 (7.8×10^{17} cm^{-3}) from 40 to 150 K, while transversal MR showed non-linearity that was attributed to the two-band conduction model [31].

In this study, the sample was measured in magnetic fields varying between −9 and +9 T and at temperature range between 2 and 200 K. The magnetoresistance is defined as $MR(B) = \frac{R(B)-R(0)}{R(0)}$, with *R(B)* the resistance value for a magnetic field *B* and *R(0)* the value at zero field. The magnetoresistance in the temperature interval of 50 to 15 K are shown in Fig. 5 (a). We observe a clear change from negative (MR < 0) to positive (MR > 0) as the temperature decreased. The negative sign of *MR* at 50 to 30 K is likely associated with the impurity conduction mechanisms, where strong localization of carriers leads to significant interaction within impurity band. While below 20 K, contribution into electrical conduction of variable range hopping (VRH) mechanism starts to increase. Interestingly, Fig. 5 (b) displays a significant increase in magnitude of positive magnetoresistance at temperatures below 10 K, reaching up to 200 % (9 T) at 2 K. In semiconductor materials under the VRH regime, the wave functions of carriers (either electrons or holes)

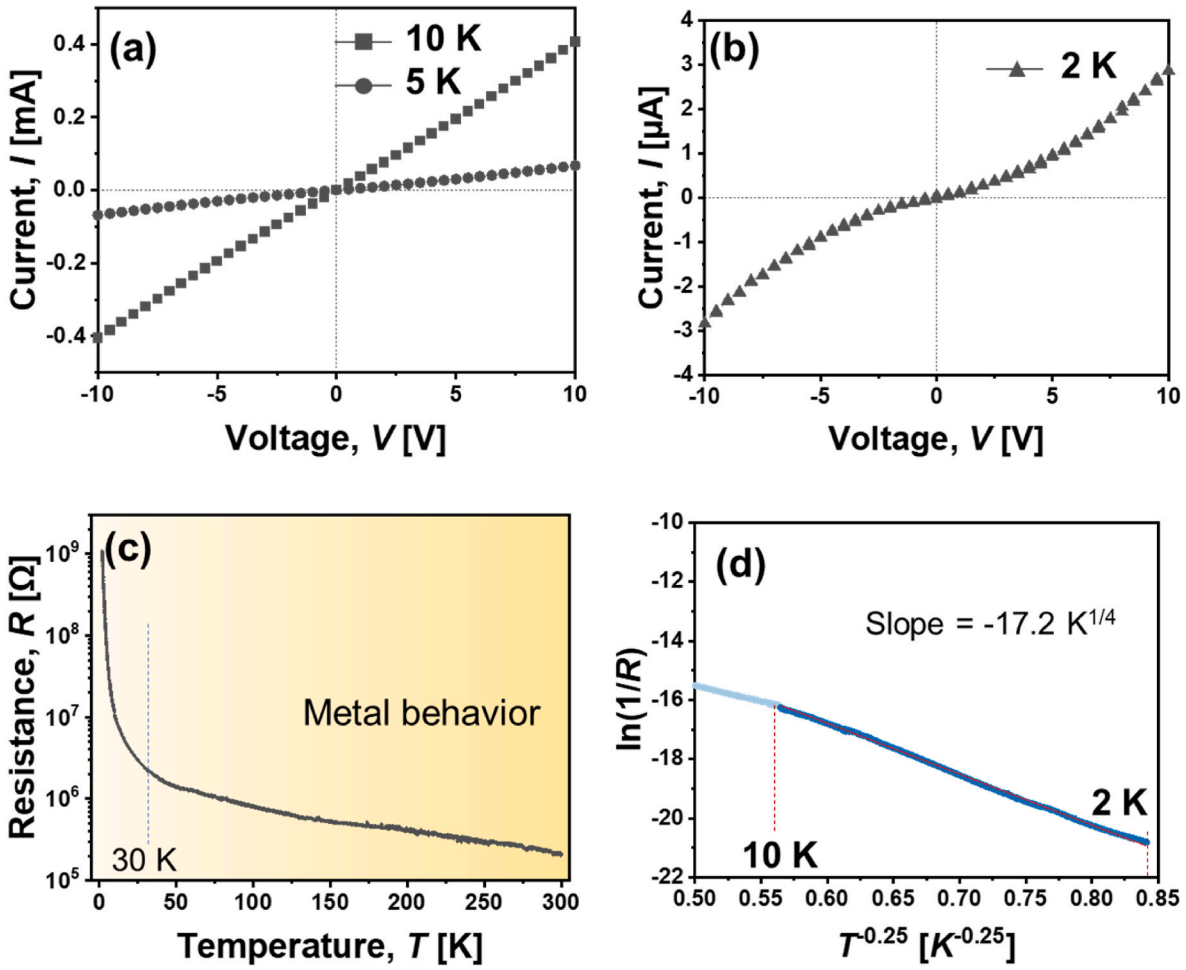

Fig. 4. (a) *I-V* characteristics at 5 and 10 K, showing an Ohmic behavior. (b) A quasi-Ohmic behavior of the *I-V* characteristics at 2 K. (c) Temperature dependent resistance in the temperature range of 2–300 K, measured by a four-point aligned configuration by PPMS. (d) Plot of ln (1/*R*) vs. $T^{-1/4}$ to fit Mott VRH model in the range of 2–10 K.

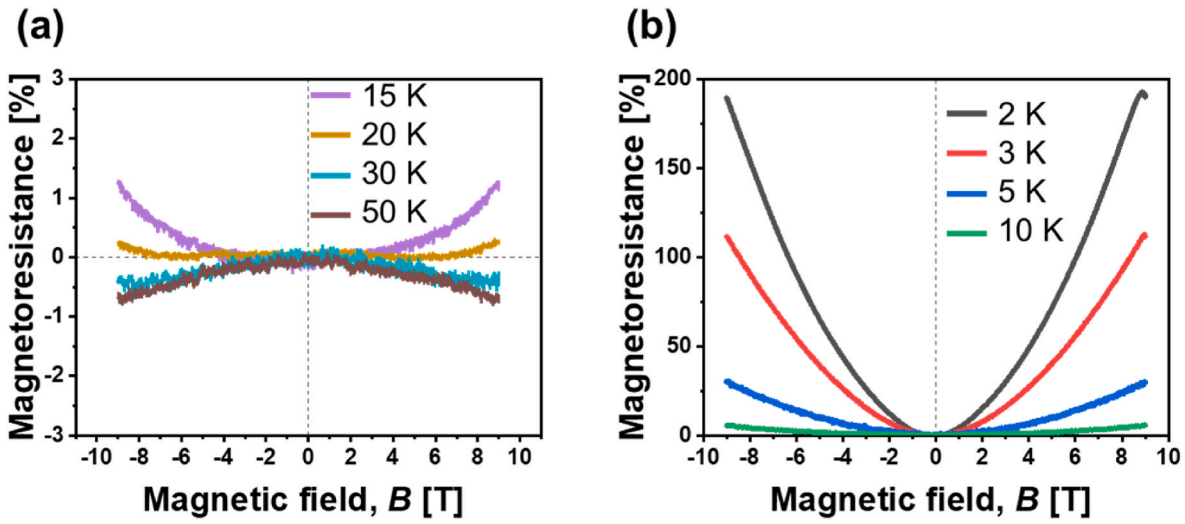

Fig. 5. Magnetoresistance vs. perpendicularly applied magnetic field (−9 – +9 T) at (a) 50–15 K, and (b) 10–2 K.

overlap. The application of the magnetic field tends to squeeze the wave functions of carriers laterally with respect to the direction of the applied magnetic field, which reduces the overlap between localized states. This reduction decreases the hopping probability, leading to an increase in resistance, hence a positive *MR* [32–34]. Such behavior has been observed in Cr doped *n*-GaAs [35], Ga doped *p*-Ge [36], with an even gigantic *MR* over several orders of magnitude. Besides, when the doping concentration is near (or higher than) the metal-insulator transition, the positive *MR* may also be attributed to the Coulomb interactions, where additional energy is required for the conduction [37,38].

2.4. Anderson model

When a material exhibits a high level of impurity incorporation coupled with significant electrical compensation ratio, two phenomena may occur: (1) impurity states can form an impurity band; (2) the electrically compensating defects with a high concentration may lead to a significant reduction of the impurity ionization energy [39]. This is caused by proximity of positively charged compensating donors. As the concentration of these compensating donors is close to that of acceptors, the average distance between them is expected to be half of the average distance between the acceptors (R). As a consequence, the ionization energy is lowered since the Coulomb repulsion energy between the bound hole and compensating donor center is given by $\frac{ze^2}{\varepsilon R/2}$. ($z$ is a charge of compensation donor; here we assume that the compensating center is the doubly charged oxygen vacancy $z = 2$).

The distance between acceptor and donor centers varies around its mean value, which causes a random variation of impurity potential, resulting in a broader impurity band in comparison with the band formed in the case of perfect periodic distribution (Fig. 6 (a)). The

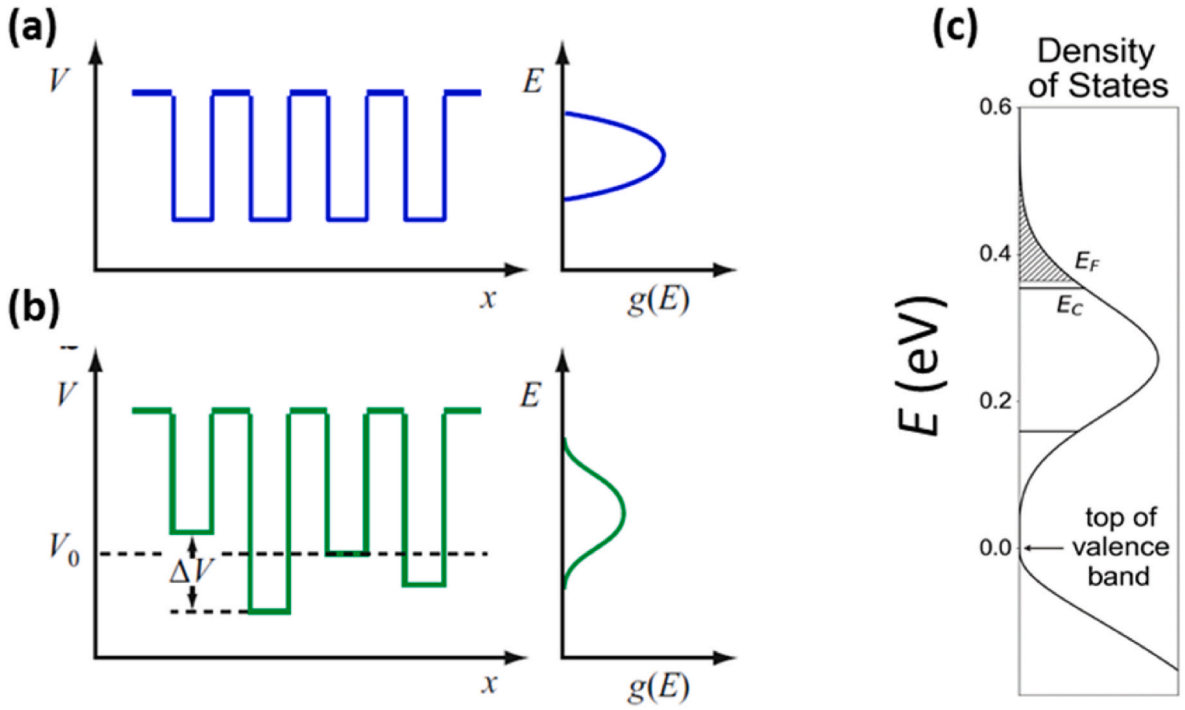

Fig. 6. (a) Anderson model for a periodic potential and resulting level distribution. (b) Anderson potential with random potential ΔV added to potential-well depth and resulting level distribution [43]. (c) Density of states inside the impurity band.

variation of impurity potential is related to the random distribution of compensating donors, which is in the range of $\sim \frac{e^2}{R}$ [40]. This random potential variation causes the formation of tails in the density of states, corresponding to localized state. These states are considered to exist above or below the critical energy E_c, also known as the mobility edge [41].

In this context, the Anderson Metal-Insulator Transition (MIT), focuses on how disorder affects the behavior of carriers, resulting in the subsequent transition [42,43]. Although the disorder can be caused by a variety of factors such as lattice defects or impurities, the Anderson model does not distinguish between specific defect types. All such defects can be treated as contributors to the random potential field that constitutes disorder in the model. Instead, doping concentration plays a critical role in Anderson localization. The MIT in the Anderson model primarily depends on the degree of disorder, and doping concentration directly modulates the disorder strength in the system [40,44].

In the case of acceptor doping, the holes occupying the states with energies above E_c (conduction band edge) are localized; while those which occupy the states with energies bellow E_c are delocalized. Therefore, when the Fermi level E_F is above E_c, most of the occupied states are localized, and the material behaves as an insulator. Conversely, when $E_F = E_c$, the Fermi level intersects the boundary between localized and delocalized states, a small change in temperature can shift the balance to the delocalized states, the metal insulator transition takes place subsequently.

To explain the experimental results, we modeled the formation of the impurity band considering the lowering of the impurity level due to compensating defects and random variation of impurity potential. Calculation details are provided in supplementary file. We estimated the electronic structure of highly P-doped gallium oxide by modeling an individual P impurity by one dimensional rectangular potential well [45]. Interactions between the impurities and random variation of potential were described by Anderson model, where the random variation of potential was modeled by variation of the depth of potential wells [46] Fig. 6 (a).

In our calculation, the depth of the potential well describing individual substitutional phosphorus was taken as 0.73 eV, which represents the difference between the electron affinities of oxygen and phosphorus atoms. This is conditioned by: (1) The difference in electron affinities between oxygen and phosphorus, which approximates the difference between the energies of electron bound to these atoms. (2) The valence band is primarily composed of O-2*p* states [47]. Both oxygen and phosphorus possess positive electron affinities, while the electron affinity of, e.g., nitrogen is negative (−0.07 eV) [48]. The differences are approximately 0.73 eV for phosphorus and 1.5 eV for nitrogen. Consequently, the energy level of substitutional phosphorus might be shallower than that of substitutional nitrogen (e.g., a N related level at E_C – 2.9 eV was found by DLOS [49]). Besides, one of the key parameters which defines the energy level of a particle confined in quantum well is its effective mass. The lighter (small effective mass) the carrier, the shallower the level. In gallium oxide, high anisotropy in the hole effective masses is expected [50]. Here, we used the effective mass $m^*_{h,dos} = \left(m^*_a m^*_b m^*_c\right)^{1/3} \approx 1.9\, m_0$, a geometrically averaged value taken from Ref. [50]. The average variation of the potential well depth is taken as 0.1 eV ($\sim \frac{e^2}{R}$, R the distance between the impurities), the quantum well width was set to 4 Å (approximately twice of the Ga-O distance of 1.83 Å [51]). Using these parameters, the estimated ionization energy of the acceptor is 0.55 eV, its reduction caused by the proximity of donors is estimated to 0.15 eV.

To account for the random variation of potential and get the density of state in the impurity band, we employed Monte Carlo simulations to statistically analyze the effects of white noise perturbations on the electronic energies. The potential was randomly generated using mean of 0 and a standard deviation represented by $\frac{e^2}{R} \approx 0.1$ eV. For each generated potential, the Schrödinger equation was numerically solved yielding a set of energies ($E1, E2, \ldots$), allowing us to construct the Probability Density Function for these energies, which in fact represents relative density of states in the case of random variation of potential. The details of calculations can be found in supplementary material. The results of calculations are given in Fig. 6 (c). The mobility edges are shown by solid lines (0.35 eV approximately), they are defined as the points where wave functions start to cover several impurity sites and carriers are strongly localized. The shaded area corresponds to the states occupied by bound holes. Lower limit of the shaded area represents the Fermi energy, which is in the range few meV away from the mobility edge. Therefore, the temperature of above 20–30 K must be enough for holes to overcome the mobility edge, consequently, metal-insulator transition could take place within this temperature range. As a result, the resistivity of the *p*-type sample is as low as 1.3 Ω cm at room temperature, despite the findings that phosphorus is not shallow in β-Ga_2O_3 according to either DFT [22,27] or our model.

At higher temperatures, one can expect the activation of holes from the Fermi level into the valence band. However, because of the interference with activation from localized to delocalized states inside the impurity band ($E_F \rightarrow E_c$) mentioned above, we did not observe the real activation energy of the process. Indeed, such impurity band conduction effects are more pronounced for deep acceptors than for shallow ones [52]. A similar scenario was reported by Rathkanthiwar et al. for Mg doped *p*-type ultra-wide band gap semiconductor AlGaN films [53]. It was proposed that, due to the presence of compensating defects in their *p*-AlGaN layers, the impurity band was disrupted. Consequently, Anderson transition takes place with a reduction of conductivity.

3. Conclusion

Phosphorus implantation has been recently reported as a novel route to achieve acceptor *p*-type conduction on Ga_2O_3 at room temperature. In this work, we first analyzed the physical properties of phosphorus ions implanted β-Ga_2O_3 (−201) epilayers grown on *c*-sapphire substrates. The transport properties of the epilayers were further investigated by means of Hall effect measurements in the 300–600 K range with $p \sim 4$–6×10^{18} cm^{-3}, $\mu = 1.2$–2.1 cm^2/(V·s), and $\rho = 1.3$–0.5 Ω cm, indicating a high level of compensation. Below 30 K, a metal-insulator transition was observed along with a positive magnetoresistance reaching up to 200 % at 9 T. To understand these behaviors, the formation of the impurity band was modeled considering an individual phosphorus impurity as one-dimensional potential well. Subsequently, the density of states was obtained using white noise perturbations in the frame of Monte Carlo simulations considering the reduction of the impurity ionization energy by compensating defects and random variation of impurity potential, with a mobility edge estimated to be approximately at $E_V + 0.35$ eV, and the Fermi level situated a few meV to the mobility edge.

In conclusion, our results suggested that the Anderson model with the proposed input parameters satisfactorily explains the experimental results: impurity conduction and the absence of band conduction observation due to tiny difference between Fermi energy and mobility edge, and the transition to insulator state caused by random variation of potential. These results are very important in the context of realization and understanding *p*-type conductivity achievement challenge in Ga_2O_3, showing that the lack of a shallow acceptor can be overcome by high level of acceptor incorporation via promoting Anderson disorder.

4. Experimental details

Sample preparation: The unintentional doped (UID) β-Ga_2O_3 epilayers were grown at 875 °C on *c*-plane (0001) sapphire substrate by MOCVD. The UID sample means the β-Ga_2O_3 epilayer did not be doped by any dopant source during the epitaxial growth. The thickness of UID β-Ga_2O_3 epilayers was about 220 nm. Triethylgallium (TEGa) and high-

purity oxygen (O_2, 99.999 %) were utilized as the precursors for gallium and oxygen, respectively. The flow rates of TEGa and O_2 were set at 100 sccm and 500 sccm, respectively, while maintaining a growth pressure of 15 Torr.

X-ray diffraction: The X-ray diffraction was used to investigate the crystalline structure of β-Ga_2O_3 films by Siemens D5000 X-ray diffractometer with Cu-Kα1 source of $\lambda = 0{,}1541$ nm, and recorded between 20° and 100° for both β-Ga_2O_3 thin layers.

Secondary-ion mass spectrometry: The secondary-ion mass spectrometry was conducted using Cameca IMS 7F SIMS instrument, for the depth profiling of elements of Ga, O, P, etc.

Optical transmittance, reflectance: Optical transmittance and reflectance spectra β-Ga_2O_3 thin films were measured in 200 – 850 nm spectral range at room temperature with a Perklin Elmer 950, 2 ways spectrophotometer.

Simulation model: We simulated a β-Ga_2O_3//Al_2O_3 structure based on the experimental structure. The thicknesses of the phosphorus implanted β-Ga_2O_3 and the Al_2O_3 substrate are simulated as 170 nm and 5 μm, respectively. 0.27 m_0 and the geometrically averaged 1.9 m_0 were taken as the effective mass of electrons and holes, respectively. The β-Ga_2O_3 epi-layer doping concentration, mobility, and bandgap are 4.4×10^{18} cm^{-3}, 1.3 $cm^2/(V{\cdot}s)$, and 4.8 eV, respectively.

Hall effect: Hall effect measurements were performed in a Van der Pauw configuration by custom designed high impedance measurement set-up with magnetic fields of -1.6 – 1.6 T perpendicular to the film plane.

Low temperature resistance measurements: The β-Ga_2O_3 epilayer with high dose was studied by the standard "resistivity" option of 9 T physical property measurement system (PPMS, Quantum Design) equipment, using the four-point aligned configuration, in the magnetic field range of -9 – +9 T, and temperature from 2 to 300 K. For high resistance measurements external electrometer was used.

CRediT authorship contribution statement

Zeyu Chi: Writing – review & editing, Writing – original draft, Methodology, Formal analysis, Data curation, Conceptualization. **Se-Rim Park:** Formal analysis, Data curation. **Luka Burdiladze:** Formal analysis. **Tamar Tchelidze:** Writing – review & editing, Formal analysis. **Jean-Michel Chauveau:** Writing – review & editing, Validation, Funding acquisition. **Yves Dumont:** Writing – review & editing, Validation. **Sang-Mo Koo:** Validation. **Zurab Kushitashvili:** Formal analysis, Data curation. **Amiran Bibilashvili:** Formal analysis, Data curation. **Gérard Guillot:** Writing – review & editing, Validation. **Amador Pérez-Tomás:** Writing – review & editing, Validation. **Xin-Ying Tsai:** Methodology. **Fu-Gow Tarntair:** Methodology. **Ray Hua Horng:** Writing – review & editing, Validation, Methodology, Investigation, Funding acquisition. **Ekaterine Chikoidze:** Writing – review & editing, Validation, Supervision, Investigation, Formal analysis, Conceptualization.

Declaration of competing interest

The authors declare that they have no known competing financial interests or personal relationships that could have appeared to influence the work reported in this paper.

Acknowledgement

The present work is a part of "GALLIA" International Research Project, CNRS, France. GEMaC colleagues acknowledge financial support of French National Agency of Research (ANR), project "GOPOWER", CE-50 N0015-01. This work was partially funded by the France 2030 programme "ANR-11-IDEX-0003″ via Integrative Institute of Materials from Paris-Saclay University - 2IM@UPSaclay. This work was partially funded by EU HORIZON-CL5-2024-D3-01 Safer and More Reliable WBG/UWBG-Based MVDC Power Converters (SAFEPOWER) 101172940. We would acknowledge: GEMaC colleagues Dr.François Jomard and Dr. Estelle Loire contribution with SIMS analysis and David Hrabovsky, Sorbonne University for the PPMS measurements. This work is partially supported by Shota Rustaveli National Science Foundation of Georgia, Grant Number STEM-22-188, the Spanish Maria de Maeztu grant CEX2023-001397-M funded by MICIU/AEI/10.13039/501100011033 and project "OptoFET" (No PID2020-117201RB-C22). This study was also supported by National Science and Technology Council, Taiwan, R.O.C., under the grants Nos: 112-2622-E-A49 -011, 112-2221-E-A49-069-MY3.

Appendix A. Supplementary data

Supplementary data to this article can be found online at https://doi.org/10.1016/j.mtphys.2024.101602.

Data availability

Data will be made available on request.

References

[1] E. Chikoidze, T. Tchelidze, C. Sartel, Z. Chi, R. Kabouche, I. Madaci, C. Rubio, H. Mohamed, V. Sallet, F. Medjdoub, A. Perez-Tomas, Y. Dumont, Ultra-high critical electric field of 13.2 MV/cm for Zn-doped p-type β-Ga2O3, Mater. Today Phys. 15 (2020): 100263, https://doi.org/10.1016/j.mtphys.2020.100263.

[2] M. Higashiwaki, K. Sasaki, A. Kuramata, T. Masui, S. Yamakoshi, Gallium oxide (Ga2O3) metal-semiconductor field-effect transistors on single-crystal β-Ga2O3 (010) substrates, Appl. Phys. Lett. 100 (2012): 013504, https://doi.org/10.1063/1.3674287.

[3] F. Alema, G. Seryogin, A. Osinsky, A. Osinsky, Ge doping of β-Ga2O3 by MOCVD, Apl. Mater. 9 (2021): 091102, https://doi.org/10.1063/5.0059657.

[4] E. Chikoidze, H.J. von Bardeleben, K. Akaiwa, E. Shigematsu, K. Kaneko, S. Fujita, Y. Dumont, Electrical, optical, and magnetic properties of Sn doped α-Ga_2O_3 thin films, J. Appl. Phys. 120 (2016): 025109, https://doi.org/10.1063/1.4958860.

[5] Z. Feng, A.F.M. Anhar Uddin Bhuiyan, M.R. Karim, H. Zhao, MOCVD homoepitaxy of Si-doped (010) β-Ga_2O_3 thin films with superior transport properties, Appl. Phys. Lett. 114 (2019): 250601, https://doi.org/10.1063/1.5109678.

[6] K. Goto, K. Konishi, H. Murakami, Y. Kumagai, B. Monemar, M. Higashiwaki, A. Kuramata, S. Yamakoshi, Halide vapor phase epitaxy of Si doped β-Ga_2O_3 and its electrical properties, Thin Solid Films 666 (2018) 182–184, https://doi.org/10.1016/j.tsf.2018.09.006.

[7] W. Zhou, C. Xia, Q. Sai, H. Zhang, Controlling n-type conductivity of β-Ga2O3 by Nb doping, Appl. Phys. Lett. 111 (2017): 242103, https://doi.org/10.1063/1.4994263.

[8] Y. Wang, Z. Lin, J. Ma, Y. Wu, H. Yuan, D. Cui, M. Kang, X. Guo, J. Su, J. Miao, Z. Shi, T. Li, J. Zhang, Y. Hao, J. Chang, Multifunctional solar-blind ultraviolet photodetectors based on p-PCDTBT/n-Ga2O3 heterojunction with high photoresponse, InfoMat 6 (2024): e12503, https://doi.org/10.1002/inf2.12503.

[9] M. Higashiwaki, K. Sasaki, T. Kamimura, M. Hoi Wong, D. Krishnamurthy, A. Kuramata, T. Masui, S. Yamakoshi, Depletion-mode Ga2O3 metal-oxide-semiconductor field-effect transistors on β-Ga2O3 (010) substrates and temperature dependence of their device characteristics, Appl. Phys. Lett. 103 (2013): 123511, https://doi.org/10.1063/1.4821858.

[10] C.-H. Lu, F.-G. Tarntair, Y.-C. Kao, N. Tumilty, R.-H. Horng, Undoped β-Ga2O3 layer thickness effect on the performance of MOSFETs grown on a sapphire substrate, ACS Appl. Electron. Mater. 6 (2024) 568–575, https://doi.org/10.1021/acsaelm.3c01558.

[11] W. Li, D. Saraswat, Y. Long, K. Nomoto, D. Jena, H.G. Xing, Near-ideal reverse leakage current and practical maximum electric field in β-Ga2O3 Schottky barrier diodes, Appl. Phys. Lett. 116 (2020): 192101, https://doi.org/10.1063/5.0007715.

[12] J. Zhang, P. Dong, K. Dang, Y. Zhang, Q. Yan, H. Xiang, J. Su, Z. Liu, M. Si, J. Gao, M. Kong, H. Zhou, Y. Hao, Ultra-wide bandgap semiconductor Ga2O3 power diodes, Nat. Commun. 13 (2022) 3900, https://doi.org/10.1038/s41467-022-31664-y.

[13] F. Zhou, H. Gong, M. Xiao, Y. Ma, Z. Wang, X. Yu, L. Li, L. Fu, H.H. Tan, Y. Yang, F.-F. Ren, S. Gu, Y. Zheng, H. Lu, R. Zhang, Y. Zhang, J. Ye, An avalanche-and-surge robust ultrawide-bandgap heterojunction for power electronics, Nat. Commun. 14 (2023) 4459, https://doi.org/10.1038/s41467-023-40194-0.

[14] E. Chikoidze, A. Fellous, A. Perez-Tomas, G. Sauthier, T. Tchelidze, C. Ton-That, T. T. Huynh, M. Phillips, S. Russell, M. Jennings, B. Berini, F. Jomard, Y. Dumont, P-type β-gallium oxide: a new perspective for power and optoelectronic devices, Mater. Today Phys. 3 (2017) 118–126, https://doi.org/10.1016/j.mtphys.2017.10.002.

[15] A.Y. Polyakov, N.B. Smirnov, I.V. Shchemerov, E.B. Yakimov, J. Yang, F. Ren, G. Yang, J. Kim, A. Kuramata, S.J. Pearton, Point defect induced degradation of electrical properties of Ga_2O_3 by 10 MeV proton damage, Appl. Phys. Lett. 112 (2018): 032107, https://doi.org/10.1063/1.5012993.

[16] A.M. Gurvich, Introduction to the Physical Chemistry of Crystal Phosphors, Moscow, 1982 (In Russian).
[17] E. Chikoidze, C. Sartel, H. Yamano, Z. Chi, G. Bouchez, F. Jomard, V. Sallet, G. Guillot, K. Boukheddaden, A. Pérez-Tomás, T. Tchelidze, Y. Dumont, Electrical properties of p-type Zn:Ga2O3 thin films, J. Vac. Sci. Technol. A 40 (2022): 043401, https://doi.org/10.1116/6.0001766.
[18] C. Ma, Z. Wu, Z. Jiang, Y. Chen, W. Ruan, H. Zhang, H. Zhu, G. Zhang, J. Kang, T.-Y. Zhang, J. Chu, Z. Fang, Exploring the feasibility and conduction mechanisms of P-type nitrogen-doped β-Ga2O3 with high hole mobility, J. Mater. Chem. C 10 (2022) 6673–6681, https://doi.org/10.1039/D1TC05324H.
[19] Z.Y. Wu, Z.X. Jiang, C.C. Ma, W. Ruan, Y. Chen, H. Zhang, G.Q. Zhang, Z.L. Fang, J. Y. Kang, T.-Y. Zhang, Energy-driven multi-step structural phase transition mechanism to achieve high-quality p-type nitrogen-doped β-Ga2O3 films, Mater. Today Phys. 17 (2021): 100356, https://doi.org/10.1016/j.mtphys.2021.100356.
[20] C. Ma, Z. Wu, H. Zhang, H. Zhu, J. Kang, J. Chu, Z. Fang, P-type nitrogen-doped β-Ga2O3: the role of stable shallow acceptor NO–VGa complexes, Phys. Chem. Chem. Phys. 25 (2023) 13766–13771, https://doi.org/10.1039/D3CP00245D.
[21] Z. Chi, C. Sartel, Y. Zheng, S. Modak, L. Chernyak, C.M. Schaefer, J. Padilla, J. Santiso, A. Ruzin, A.-M. Gonçalves, J. von Bardeleben, G. Guillot, Y. Dumont, A. Pérez-Tomás, E. Chikoidze, Native defects association enabled room-temperature p-type conductivity in β-Ga2O3, J. Alloys Compd. 969 (2023): 172454, https://doi.org/10.1016/j.jallcom.2023.172454.
[22] L. Li, F. Liao, X. Hu, The possibility of N–P codoping to realize P type β-Ga_2O_3, Superlattices Microstruct 141 (2020): 106502, https://doi.org/10.1016/j.spmi.2020.106502.
[23] R.H. Horng, X.-Y. Tsai, F.-G. Tarntair, J.-M. Shieh, S.-H. Hsu, J.P. Singh, G.-C. Su, P.-L. Liu, P-type conductive Ga2O3 epilayers grown on sapphire substrate by phosphorus-ion implantation technology, Mater. Today Adv. 20 (2023): 100436, https://doi.org/10.1016/j.mtadv.2023.100436.
[24] C.-Y. Huang, X.-Y. Tsai, F.-G. Tarntair, C. Langpoklakpam, T.S. Ngo, P.-J. Wang, Y.-C. Kao, Y.-K. Hsiao, N. Tumilty, H.-C. Kuo, T.-L. Wu, C.-L. Hsiao, R.-H. Horng, Heteroepitaxially grown homojunction gallium oxide PN diodes using ion implantation technologies, Mater. Today Adv. 22 (2024): 100499, https://doi.org/10.1016/j.mtadv.2024.100499.
[25] R. Lingaparthi, K. Sasaki, Q.T. Thieu, A. Takatsuka, F. Otsuka, S. Yamakoshi, A. Kuramata, Surface related tunneling leakage in β-Ga2O3 (001) vertical Schottky barrier diodes, Appl. Phys. Express 12 (2019): 074008, https://doi.org/10.7567/1882-0786/ab2824.
[26] K. Matsuzawa, K. Uchida, A. Nishiyama, A unified simulation of Schottky and ohmic contacts, IEEE Trans. Electron Devices 47 (2000) 103–108, https://doi.org/10.1109/16.817574.
[27] C.J. Zeman, S.M. Kielar, L.O. Jones, M.A. Mosquera, G.C. Schatz, Investigation of p-type doping in β- and κ-Ga2O3, J. Alloys Compd. 877 (2021): 160227, https://doi.org/10.1016/j.jallcom.2021.160227.
[28] N.F. Mott, Conduction in non-crystalline materials: III. Localized states in a pseudogap and near extremities of conduction and valence bands, Philos. Mag. J. Theor. Exp. Appl. Phys. 19 (1969) 835–852, https://doi.org/10.1080/14786436908216338.
[29] V. Ambegaokar, B.I. Halperin, J.S. Langer, Hopping conductivity in disordered systems, Phys. Rev. B 4 (1971) 2612–2620, https://doi.org/10.1103/PhysRevB.4.2612.
[30] N.F. Mott, E.A. Davis, Electronic Processes in Non-crystalline Materials, OUP Oxford, 1979.
[31] A.K. Rajapitamahuni, L.R. Thoutam, P. Ranga, S. Krishnamoorthy, B. Jalan, Impurity band conduction in Si-doped β-Ga2O3 films, Appl. Phys. Lett. 118 (2021): 072105, https://doi.org/10.1063/5.0031481.
[32] S. Ding, C. Jin, Z. Fan, P. Li, H. Bai, Sign change of magnetoresistance in Gd-doped amorphous carbon granular films, Phys. Chem. Chem. Phys. 17 (2015) 30695–30701, https://doi.org/10.1039/C5CP05070G.
[33] J.J.H.M. Schoonus, P.P.J. Haazen, H.J.M. Swagten, B. Koopmans, Unravelling the mechanism of large room-temperature magnetoresistance in silicon, J. Phys. Appl. Phys. 42 (2009): 185011, https://doi.org/10.1088/0022-3727/42/18/185011.
[34] J.J.H.M. Schoonus, F.L. Bloom, W. Wagemans, H.J.M. Swagten, B. Koopmans, Extremely large magnetoresistance in boron-doped silicon, Phys. Rev. Lett. 100 (2008): 127202, https://doi.org/10.1103/PhysRevLett.100.127202.
[35] H. Kahlert, G. Landwehr, A. Schlachetzki, H. Salow, Impurity conduction and magnetoresistance in lightly dopedn-type GaAs, Z. Für Phys. B Condens. Matter 24 (1976) 361–365, https://doi.org/10.1007/BF01351525.
[36] W.W. Lee, R.J. Sladek, Hop-conduction magnetoresistance in p-Type germanium, Phys. Rev. 158 (1967) 794–798, https://doi.org/10.1103/PhysRev.158.794.
[37] A.V. Nenashev, F. Jansson, M. Wiemer, S. Petznick, P.J. Klar, M. Hetterich, A. V. Dvurechenskii, F. Gebhard, S.D. Baranovskii, Scaling approach to hopping magnetoresistivity in dilute magnetic semiconductors, Phys. Rev. B 88 (2013): 115210, https://doi.org/10.1103/PhysRevB.88.115210.
[38] T.F. Rosenbaum, R.F. Milligan, M.A. Paalanen, G.A. Thomas, R.N. Bhatt, W. Lin, Metal-insulator transition in a doped semiconductor, Phys. Rev. B 27 (1983) 7509–7523, https://doi.org/10.1103/PhysRevB.27.7509.
[39] B. Podor, Thermal ionization energy of Mg acceptors in GaN: effects of doping level and compensation, in: Int. Conf. Solid State Cryst. 2000 Growth Charact, Appl. Single Cryst., SPIE, 2001, pp. 299–303, https://doi.org/10.1117/12.435848.
[40] N.F. Mott, Impurity band conduction. Experiment and theorythe metal-insulator transition in an impurity band, J. Phys. Colloq. 37 (1976) C4–C306, https://doi.org/10.1051/jphyscol:1976453.
[41] N.F. Mott, Metal-insulator transition, Rev. Mod. Phys. 40 (1968) 677–683, https://doi.org/10.1103/RevModPhys.40.677.
[42] P.W. Anderson, Absence of diffusion in certain random lattices, Phys. Rev. 109 (1958) 1492–1505, https://doi.org/10.1103/PhysRev.109.1492.
[43] F. Evers, A.D. Mirlin, Anderson transitions, Rev. Mod. Phys. 80 (2008) 1355–1417, https://doi.org/10.1103/RevModPhys.80.1355.
[44] B. Kramer, A. MacKinnon, Localization: theory and experiment, Rep. Prog. Phys. 56 (1993) 1469, https://doi.org/10.1088/0034-4885/56/12/001.
[45] K.W. Böer, U.W. Pohl, Superconductivity, in: K.W. Böer, U.W. Pohl (Eds.), Semicond. Phys., Springer International Publishing, Cham, 2018, pp. 993–1016, https://doi.org/10.1007/978-3-319-69150-3_26.
[46] K.W. Böer, U.W. Pohl, Defects in amorphous and organic semiconductors, in: K. W. Böer, U.W. Pohl (Eds.), Semicond. Phys., Springer International Publishing, Cham, 2018, pp. 781–812, https://doi.org/10.1007/978-3-319-69150-3_20.
[47] Y. Zhang, M. Liu, D. Jena, G. Khalsa, Tight-binding band structure of β- and α-phase Ga2O3 and Al2O3, J. Appl. Phys. 131 (2022): 175702, https://doi.org/10.1063/5.0074598.
[48] S.G. Bratsch, J.J. Lagowski, Predicted stabilities of monatomic anions in water and liquid ammonia at 298.15 K, Polyhedron 5 (1986) 1763–1770, https://doi.org/10.1016/S0277-5387(00)84854-8.
[49] H. Ghadi, J.F. McGlone, E. Cornuelle, A. Senckowski, S. Sharma, M.H. Wong, U. Singisetti, Y.K. Frodason, H. Peelaers, J.L. Lyons, J.B. Varley, C.G. Van de Walle, A. Arehart, S.A. Ringel, Identification and characterization of deep nitrogen acceptors in β-Ga2O3 using defect spectroscopies, Apl. Mater. 11 (2023): 111110, https://doi.org/10.1063/5.0160541.
[50] A. Mock, R. Korlacki, C. Briley, V. Darakchieva, B. Monemar, Y. Kumagai, K. Goto, M. Higashiwaki, M. Schubert, Band-to-band transitions, selection rules, effective mass and exciton binding energy parameters in monoclinic \beta-Ga2O3, Phys. Rev. B 96 (2017): 245205, https://doi.org/10.1103/PhysRevB.96.245205.
[51] S. Geller, Crystal structure of β-Ga2O3, J. Chem. Phys. 33 (1960) 676–684, https://doi.org/10.1063/1.1731237.
[52] H. Neumann, Influence of impurity band conduction on the electrical characteristics of p-type GaAs, Cryst. Res. Technol. 23 (1988) 1377–1383, https://doi.org/10.1002/crat.2170231032.
[53] S. Rathkanthiwar, P. Reddy, C.E. Quiñones, J. Loveless, M. Kamiyama, P. Bagheri, D. Khachariya, T. Eldred, B. Moody, S. Mita, R. Kirste, R. Collazo, Z. Sitar, Anderson transition in compositionally graded p-AlGaN, J. Appl. Phys. 134 (2023): 195705, https://doi.org/10.1063/5.0176419.